Numerical Simulations of Coarsening of Lamellar Structures: Applications to metallic alloys

Rifa J. El-Khozondar [1], Hala J. El-Khozondar [2]

[1] Department of Physics, Al-Aqsa University, Gaza
[2] Department of Electrical Engineering, Islamic University, Gaza

Understanding the microstructural evolution in metallic alloys helps to control their properties and improve their performance in industrial applications. The emphasis of our study is the coarsening mechanisms of lamellar structures. Coarsening of lamellar structure is modeled numerically using Monte Carlo Potts method. The initial microstructure consists of alternating lamellae of phase A and phase B with the spacing proportional to their volume fraction. Faults are introduced to the lamellae to induce instability in the system. We find that an isotropic lamellar structure degenerates via edge spheroidization and termination migration into nearly equiaxed grains with a diameter which is 2 to 3 times larger than the original lamellar spacing. The duration of this process is comparable with the time it would take Ostwald ripening to produce grains of the same size. Eventually grain growth reaches the asymptotic regime of coarsening described by a power-law function of time. Lamellae with anisotropic grain boundaries coarsen more slowly and via discontinuous coarsening mechanism. This produces larger grains upon degeneration of lamellae. Discontinuous coarsening was observed in lamellar alloys as well as termination migration.

1. Introduction:

Microstructural evolution due to aging determines the long-term reliability of materials in practical applications. The ability to control the properties of materials and enhance their performance depends upon the development of material models. Various numerical models have been developed to simulate the microstructural evolution of materials. The simulation methods can be classified into four specific groups [1]. The first one is made up of Voronoi [2] and modified Voronoi [3, 4] methods. The second contains curvature-driven grain growth [5 - 8] simulations, followed by continuum thermodynamics methods such as finite different solutions of the

Cahn-Hilliard equation, phase field models [9], and diffusion equation [10 - 12]. The last one consists of cellular automata models. Each of these simulations will be summarized briefly.

Voronoi and modified Voronoi techniques simulate grain microstructures in two dimensions by defining nucleation rates and grain boundary velocity. The nucleated grain growth continues until the grains impinge on other growing grains. Although theses methods are applicable to the study of nucleation and growth conditions, they fail to give kinetic information.

Curvature-driven grain growth simulations are based on the relationship between the grain boundary curvature and its velocity. In this method, discrete segments of the grain boundary are moved with velocities proportional to their curvature. Line tension and vertex driven techniques [13] suppose straight line boundaries which exert a force proportional to their length at vertices. The vertices move as a result of the total line tension force acting on them. Although this method is successful at modeling normal grain growth, it fails to model Ostwald ripening or grain growth in the presence of temperature gradients.

Continuum thermodynamic models have been successful for simulating several microstructural evolution problems; however, all thermodynamic and kinetic characteristics must be modified into the model.

Cellular automata models utilize a pixilated microstructure. The local structure change depends on the state of pixels near the considered pixel. This method requires the development of rules based on observed phenomenological characteristics.

All four simulation methods depend on knowing the system's phenomenological characteristics. In comparison, the thermodynamic and kinetic characteristics are inherent to the Monte Carlo Potts model. There is no need to incorporate the material behavior such as velocity of grain boundary or the function of free energy into the model. This model was developed for one-phase systems, two-phase solid-liquid systems and two-phase solid-solid systems [14 - 17].

In the present study, the coarsening behavior of lamellar structure of metallic alloys is simulated using the Monte Carlo Potts Model. These alloys are important for high-temperature engineering applications. For example, Sn-Pb alloys are widely used as soldering materials in the packages of semiconductors and communication materials [18]. Moreover, they are used in printed circuits and they are applied in interconnections of Si chip-to-substrates such as the multichip modules, the thermal conduction module and the tap-

automated-bonding [19]. The simulation results of both isotropic and anisotropic coarsening of lamellar structure are discussed and compared to each other and to simulation results of fine-grained structure of metallic alloys.

2. Different Mechanisms Of Grain Growth:

Most metallic alloys are polycrystalline materials which consist of small grains which are "glued" together by interatomic forces. In single-phase alloys grains are attached by grain boundaries. In two-phase alloys grains of different phases are adjoined by interphase boundaries. Polycrystals are intrinsically unstable. The instability is introduced by grain boundary curvatures which lead to grain boundary migration. This boundary migration leads to minimization of interfacial energy and increasing the grain size. The grains grow via several mechanisms described as follows.

2.1. One-phase alloys

In single-phase alloys the grain boundary velocity $v \sim \dot{d}$ is proportional to the driving force P (free energy difference across curved interfaces). Assuming that P is proportional to the grain size: $P \alpha d^{-1}$, we get $d \sim t^{1/2}$. This shows that the "classical" value of grain growth exponent for pure metals or ceramics is 2 [20 - 22].

Much larger grain growth exponents, sometimes observed in laboratory experiments [23, 24] are believed to be due to non-linear relationship between the boundary velocity and the driving force, $v \alpha P^m$, where m is a constant [23]. This gives a more general result n=m+1. For example, in the case of aluminium, $m \approx 12$ at $T=0.4T_m$, and approaches m=1 as the temperature approaches melting temperature.

Impurities is another which can increase n [25]. They tend to concentrate in the moving grain boundaries affecting the driving force and therefore the grain growth rate.

2.2. Two-phase alloys:

Before a discussion of two-phase systems, we would like to note that the term "grain growth" is traditionally used for one-phase systems where grains grow via grain boundary migration. Growth of second-phase particles is usually referred to as "coarsening" or "Ostwald ripening". Sometimes, especially when both grain growth and coarsening take place at the same time, the term "grain growth" and "coarsening" are used in a broader sense.

The coarsening exponent for Ostwald ripening of particles in polycrystalline matrix is n=3 in case of volume diffusion controlled growth [26,27], n=4 if the grain growth is controlled by grain boundary diffusion [28] and n=5 for diffusion on dislocations [28].

Grain growth in the major phase often occurs simultaneously with Ostwald ripening. The coupling between the two processes can be described as follows. If the second-phase particles were stable, grain growth in the major phase will stop as soon as the grain size reaches some maximum value which is proportional to the size of the particles (Zener pinning, see [29]). If the second-phase particles undergo Ostwald ripening, the grains of the major phase can grow as well. Hillert [30] and Gladman [31] proposed that after a sufficiently long time, grain growth in two-phase systems in which both phases grow simultaneously is controlled by Ostwald ripening of the dispersed particles and is coupled through Zener pinning. There is evidence for such coupled growth in laboratory experiments [32 - 39] and in numerical simulations [40, 17]. The grain growth exponents for both phases are the same and correspond to one of the three mechanisms of Ostwald ripening described above.

3. Review Of Coarsening Mechanisms:

3.1. Direct cylinderization:

The direct cylinderiztion process is driven by the curvature between the plate edge and the flat surface. During this process, mass transfer from the edge to the flat surface produces ridges. As a result of that additional transfer of mass the ridges grow together into a circular cylinder. If the mass transfer is controlled by volume diffusion, then the cylinders grow by Ostwald ripening, in which large cylinders grow more at the expense of smaller ones. However, if the mass transfer is controlled by interfacial diffusion, then each cylinder is subject to a Rayleigh instability of sufficient wavelength along its length and will break up into a row of spheres [41].

3.2. Edge spheroidization:

Finite plates with large aspect ratios are susceptive to this kind of instability. This process starts with edge recession and the formation of ridges similar to the direct cylinderization process. Edge recession drives the ridge growth and also gives sufficient time for the development and growth of the perturbations along the ridge length. At sufficiently large wavelength of perturbations, the radius of curvature of the ridge is unstable against the perturbations. This develops the perturbations growth and eventually leads to the decomposition into a row of spheres.

3.3. Thermal groove theory:

Thermal groove due to the presence of sub-boundaries in the lamellae is another type of instability. These sub-boundaries can be introduced into the lamellar structure by deformation or phase transformation processes. Mullins [42, 43] developed the theory of thermal grooving for an internal grain boundary that intersects an interface interphase. Initially, a local equilibrium will be established at each of the triple junctions by balancing the interfacial tensions. This introduces curvatures into the lamellar interfaces and chemical potential gradients. Diffusion of atoms leaving the curved groove is controlled by these gradients. This will cause the grooves to grow, and eventually the lamellar plates break up. If the ratio of the subboundary and phase boundary energy is large, then the thermal groove mechanism (boundary splitting) dominates. However, small values of this ratio favor cylinderization. Also, large aspect ratios favor boundary splitting.

3.4. Fault migration theory:

Cline [44] discussed the role of faults in the rod composite. These faulted rods include two kinds of faults: terminations which decrease the number of the rods during growth and branches which increase the number of rods. The surface curvature is a maximum at the termination and a minimum at the branch. Diffusion of rod atoms is driven by chemical potential due to curvature differences between the branch and the termination. The terminations and the faults migrate in opposite directions so that they may collide, which cause the elimination of both faults. While the faults migrate toward each other, the rods left behind become bulged to conserve materials. Both types of faults were observed in a NiAl-Cr eutectic [44] and in an Al_3 Ni-Al eutectic [45].

3.5. Discontinuous coarsening:

Discontinuous coarsening occurs by grain boundary migration leaving a coarser lamellar structure. Discontinuous coarsening is expected to be more dominant at lower temperatures and thinner lamellar spacing. Discontinuous coarsening was observed in Co-Si, Cu-In and Ni-In [46] and TiAl/Ti_3 Al [47, 48, 49].

4. Role of Initial Conditions:

Initial conditions and inadequate coarsening time could also be the reason of an unusual large value of n. For example, a thin initial particle size can significantly slow down the coarsening rates in the early stages of Ostwald ripening [50]. Evolution of Eutectoid structure is an even more complicated process. They experience diverse morphological changes before nearly

equiaxed grains develop and conventional Ostwald ripening is established [41, 47, 51 - 54]. Additional complications are due to the fact that crystallographic orientations of lamellar are usually not random but such as to minimize the surface energy [52, 55]. This contributes substantially to the stability of eutectoid structures and can also affect Ostwald ripening after degeneration of lamellae. It is unclear if the asymptotic regime of conventional Ostwald ripening has ever been reached in any laboratory experiments on coarsening of eutectoid structures and it is indistinguishable if it happened in Yamazaki et al.'s experiments [56]. An indirect indication that the lamellar structures generated by an eutectoid phase transformation is rather a special type of initial conditions (including geometry, elastic stress, and crystallographic orientations) is that coarsening in an analogue aggregate, $CaTiO_3$-FeO, which was produced mechanically showed "normal" values of n, from 2.2 to 3.5 [57].

5. Numerical Simulations:

5.1. The model:

Coarsening of eutectoid lamellae with isotropic or anisotropic grain boundary energies in metallic alloys is systematically investigated with the help of Monte Carlo Potts model [1, 14 - 17, 58, 59]. The model has to be modified to simulate correctly coarsening of anisotropic grains. The problem is that without any modification of the numerical algorithm, dissolution of anisotropic grains produces anisotropic migrating atoms which is physically meaningless (and also gives meaningless results). To solve this problem the dissolved atoms need to be treated as follows.

Each site is given a random number (spin) between 1 and Q-1. If a site represents a dissolved atom (it is surrounded by sites of the other phase) it is given spin Q=100 or -100 depending on which phase it belongs to. In isotropic coarsening, the grain boundary energies are the same. Thus, for any pair of sites, different spins result in an interfacial energy of unity and same spins result in an interfacial energy of zero. In anisotropic coarsening, the grain boundary energies are not the same. In our model the energy of the vertical boundary is three times the energy of the horizontal boundary. Since single lattice sites have only one state, they coalesce when they meet single lattice site of the same phase. If a dissolved atom of one phase touches a grain or single site of the other phase, then the spin exchange rule is applied. If it touches a grain of the same phase, then the spin flip rule is applied.

The simulations presented in this paper were initialized using 400×400 site square lattice. Each of the 160,000 lattice sites images a group of atoms

with a unique orientation (spin). The total number of spins used in all our simulations was Q=100. The initial microstructure used in this study was generated by arranging a stack of alternating parallel lamellae of phase A and phase B with spacing proportional to the volume fraction of both phases. Faults are introduced to the lamellae to induce instability in the system. The resulting microstructure is referred to as lamellar structure.

5.2. Simulation results:

Lamellae with isotropic grain boundaries coarsen via termination migration and edge spheroidization mechanisms into nearly equiaxed grains [58]. Figure (1) is a plot of the average grain area as a function of time when the volume fraction of the second phase (phase B) is 30% and 50%. We see that the average grain area decreases as the lamellar degenerate. When the grain area reaches its minimum value, the lamellae are completely replaced by equiaxed grains whose sizes are determined by taking the square root of the grain area. The grain size of the degenerated lamellae is 2 to 3 times larger than the initial lamellar spacing weakly depending on the distance between faults. The duration of the degeneration process is comparable with the time it would take the conventional Ostwald ripening to form grains of similar size starting with negligibly small grains. After degeneration of lamellar structure, the equiaxed grains display grain growth and quickly reach the asymptotic regime described by the power law function $d \sim t^{1/4}$. These results have no dependence on the volume fraction of the second phase (phase B).

Lamellae with anisotropic grain boundaries coarsen more slowly and via a different mechanism, discontinuous coarsening. The average grain area is plotted in Fig. (2) as a function of time. The grain size of the degenerated lamellae is 4 to 5 times larger than the original lamellar spacing. The coarsening is very slow compared with coarsening of lamellar with isotropic grain boundaries.

6. Conclusion:

The grain size of degenerated lamellae of phase A and phase B in metallic alloys is about 2 to 3 times larger than the initial lamellar spacing. The duration of this process is comparable with the time it would take Ostwald ripening to form grains of the same size starting with fine-grained structure. After degeneration of lamellae the grain growth quickly reaches the asymptotic regime of Ostwald ripening. Lamellae with anisotropic grain boundaries coarsen much slower and produce larger grains upon degeneration of lamellae (by a factor of 2).

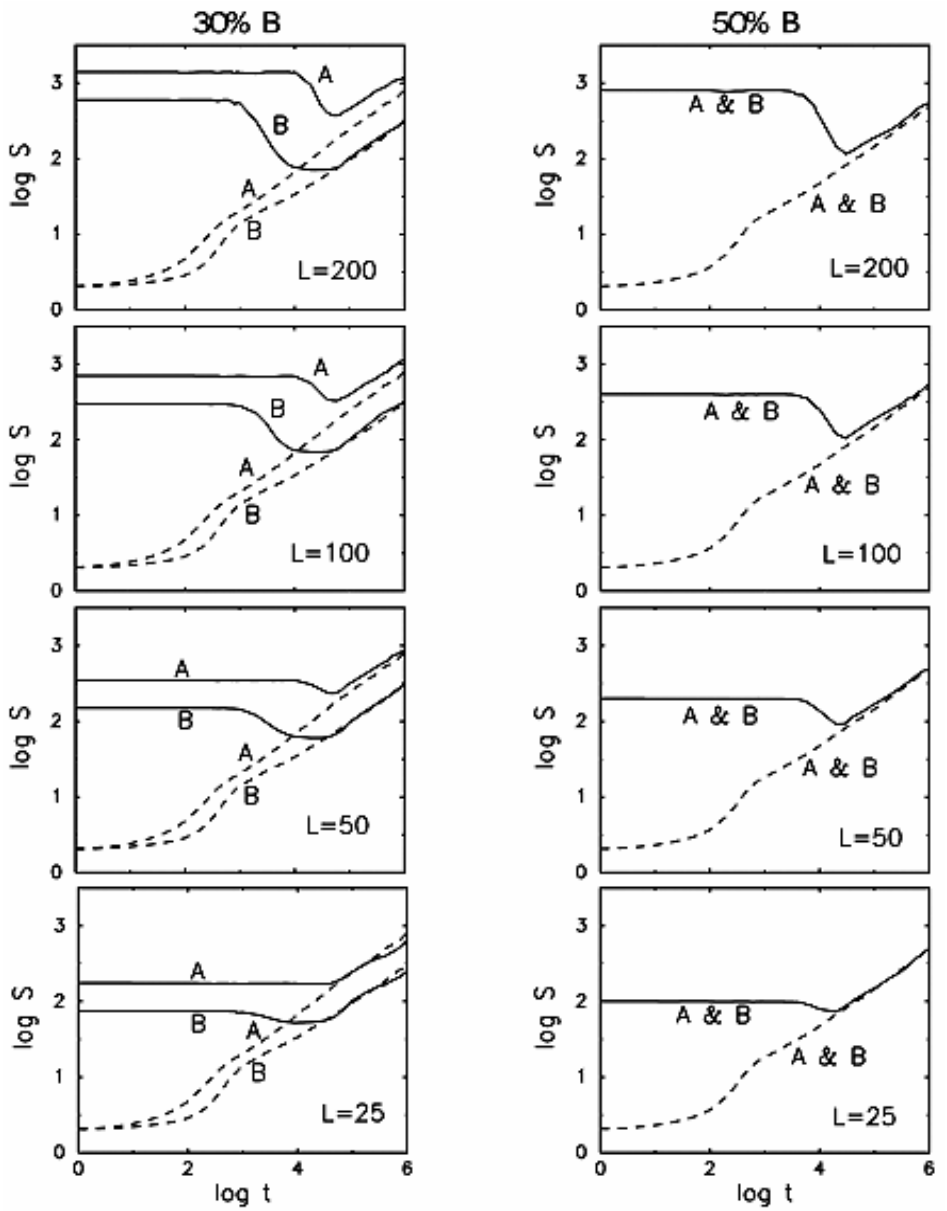

Fig.(1): The mean grain area as a function of time for isotropic boundaries. The volume fraction of the second phase is 30% and 50%. The solid lines indicate coarsening of eutectoid lamellar structure with isotropic grain boundary energies. The dotted lines indicate grain growth in two-phase systems of isotropic grain boundaries starting with small grains. L is the horizontal distance between faults in cell units. A and B stand for the first phase (phase A) and the second phase (phase B) respectively.

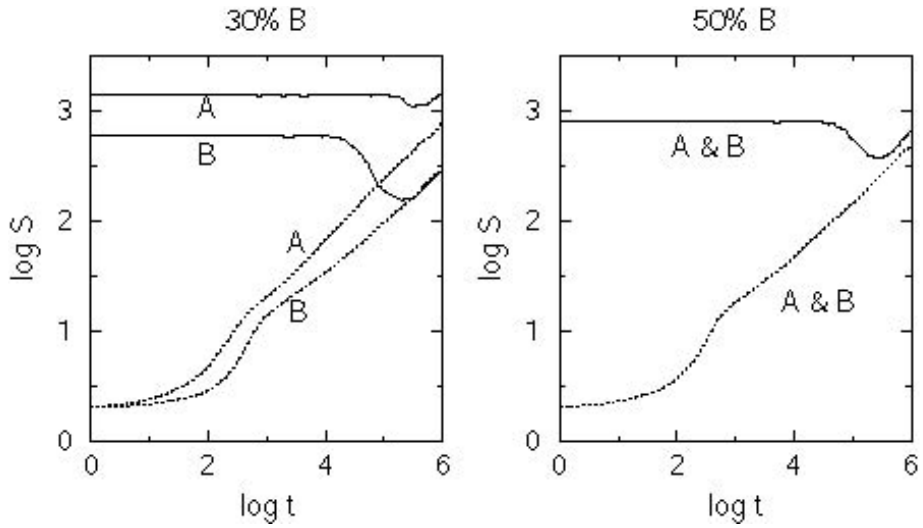

Fig.(2): The average grain area as a function of time for anisotropic boundaries. The volume fraction of the second phase is 30% and 50%. The solid lines indicate coarsening of eutectoid lamellar structure with anisotropic grain boundary energies. The dotted lines indicate grain growth in two-phase systems of isotropic grain boundaries starting with small grains. The horizontal distance between faults is L=200. A and B stand for the first phase (phase A) and the second phase (phase B), respectively.

References:

1. V. Tikare and J. D. Gawley, *J. Am. Ceram. Soc.* **81**, 485-491 (1998a).

2. K.W. Mahis, K. Hanson and J. W. Morrid Jr., *Acta Metall.* **28**, 443-453 (1980).

3. H. J. Frost and C. V. Thompson, *Acta Metall.* **35**, 529-540 (1987).

4. O. Ito and E. R. Fuller Jr., *Acta Metall.* **41**, 191-198 (1993).

5. E. Schule, *Comput. Mater. Sci.* **5**, 277-285 (1996).

6. H. J. Frost, C. V. Thompson, C. L. Howe and J. Whang, *Scr. Metal.* **22**, 65-70 (1988).

7. J. M. Chaix, M. Guyon, J. Rodriguez and C. H. Allibert, *Scr. Metal.* **22**, 71-76 (1988).

8. E. A. Ceppi and B. O. Nasello, *Scr. Metal.* **12**, 1221-1225 (1984).

9. D. Fan and L. Q. Chen, *J. Am. Ceram.* **78**, 1680-1686 (1995).

10. Z. Nikolic and W. Huppmann, *Acta Metall.* **28**, 475-479 (1980).

11. P. W. Voorhees and M. E. Glicksman, *Acta Metall.* **32**, 2001-2011 (1984).

12. P. W. Voorhees and M. E. Glicksman, *Acta Metall.* **32**, 2013-2030 (1984).
13. M. A. Fortes and A. C. Ferro, *Acta Metall.* **33**, 1697-1708 (1985).
14. M. P. Anderson, D. J. Srolovitz, G. S. Grest and P. S. Sahni, *Acta Metall.* **32**, 783-791 (1984).
15. M. P. Anderson, G. S. Grest and D. J. Srolovitz, *Phil. Mag.* **59B**, 293-329 (1989).
16. V. Tikare and J. D. Gawley, *Acta Mater.* **46**, 1343-1356 (1998b).
17. V. S. Solomatov, R. El-Khozondar, V. Tikare, *Phys. Earth Planet. Inter.* **129,** 265-282 (2002).
18. Y. L. Shen, W. Li and H. E. Fang, *Transaction of ASME* **123**, 74-78 (2001).
19. D. Gupta, K. Vieregge and W. Gust, *Acta Mater.* **47**, 5-12 (1999).
20. P. A. Beck, J. C. Kremer, L. J. Demer and M. L. Holzworth, *Trans. AIME,* **175**, 372-394 (1948).
21. J. E. Burke, *Trans. Metall. Soc. AIME,* **180**, 73-91 (1949)
22. J. E. Burke and D. Turnbull, *Prog. Metal. Phys.*, **3**, 220-292 (1952).
23. H. Hu and B. B. Rath, *Metall. Trans.*, **1**, 3181-3184 (1970).
24. G. T. Higgins, *Metal Sci.* **8**, 143-150 (1974).
25. P. Gordon, *Trans. Met. Soc. AIME* **227**, 699-705 (1963).
26. I. M. Lifshitz and V. V. Slyozov, *J. Phys. Chem. Solids*, **19**, 35-50 (1961).
27. C. Wagner, *Electrochem.* **65**, 581-591 (1961).
28. A. J. Ardell, *Acta Metall.* **20**, 601-609 (1972).
29. C. S. Smith, *Trans. AIME* **175**, 15-51 (1948).
30. M. Hillert, *Acta Metall.* **13**, 227-238 (1965).
31. T. Gladman, *Proc. R. Soc. London* **294A**, 298-309 (1966).
32. K. Mader and E. Hornbogen, *Scripta Metall.* **8**, 979-984 (1974).
33. K. Holm, J. D. Embury and G. R. Purdy, *Acta Metall.* **25**, 1191-1200 (1977).
34. G. Grewal and S. Ankem, *Metall. Trans.* **20A**, 39-54 (1989).
35. G. Grewal and S. Ankem, *Metall. Trans.* **21A**, 1645-1654 (1990a).
36. G. Grewal and S. Ankem, *Acta Metall.* **38**, 1607-1617 (1990a).
37. G. T. Higgins, S. Wiryolukito and P. Nash, *Mater. Sci. Forum* **92-96**, 671-676 (1992).
38. S. Ankem, *Mater. Sci. Forum* **92-96**, 159-168 (1992).
39. K. B. Alexander, P. F. Becher, S. B. Waters and A. Bleier, *J. Am. Ceram. Soc.* **77**, 939-946 (1994).
40. D. Fan, L. Q. Chen and S. P. P. Chen, *J. Am. Ceram. Soc.* **81**, 526-532 (1998).

41. G. Sharma, R. V. Ramanujan and G. P. Tiwari, *Acta Mater.* **48**, 875-889 (2000).
42. W. W. Mullins, *J. Appl. Phys.* **28**, 333-339 (1957).
43. W. W. Mullins, *Trans. AIME* **218**, 354-361 (1960).
44. H. E. Cline, *Acta Metall.* **19**, 481-490 (1971).
45. Y. G. Nakagawa and G. C. Weatherly, *Acta Metall.* **20**, 345-350 (1972).
46. J. D. Livingston and J. W. Cahn, *Acta Metall.* **22**, 495-503 (1974).
47. M. F. Bartholomeusz and J. A. Wert, *Metall. Mater. Trans. A.* **25A,** 2371-2381 (1994).
48. R. V. Ramanujan, P. J. Maziasz and C. T. Liu, *Acta Mater.* **44**, 2611-2642 (1996).
49. S. Mitao and L. A. Bendersky, *Acta Mater.* **45**, 4475-4489 (1997).
50. Z. G. Fang and B. R. Patterson, *Acta Metall*. **41**, 2017-2024 (1993).
51. L. D. Graham and R. W. Kraft, *Trans. Metall. Soc. AIME* **236**, 94-102 (1966).
52. G. C. Weatherly, "Treatise on Material Science and Technology," The stability of eutectic microstructures at elevated temperatures (Academic Press, 1975) pp. 121-175.
53. S. Chattopadhyay and C. M. Sellars, *Acta Metall.* **30**, 157-170 (1982).
54. M. J. Whiting and P. Tsakiropoulos, *Acta Mater.* **45**, 2027-2042 (1997).
55. J. W. Martin, R. D. Doherty and B. Cantor, "Stability of Microstructure in Metallic Systems," (Cambridge University Press, 1997).
56. D. Yamazaki, T. Kato, E. Ohtani and M. Toriumi, *Science* **274**, 2052-2054 (1996).
57. Z. C. Wang, S. Mei, S. Karato and R. Wirth, *Phys. Chem. Miner.* **27**, 11-19 (1999).
58. R. El-Khozondar, V. S. Solomatov, V. Tikare, *Mat. Res. Soc. Symp. Proc.* **731**, 1-6 (2002).
59. V. Tikare, E. A. Holm, D. Fan, L. Q. Chen, *Act Mater* **47,** 363-371.